Dalton Transactions

PAPER

View Article Online
View Journal

Cite this: DOI: 10.1039/d6dt00742b

A trifunctional cyclohexasilane for branched poly(cyclosilane)s

Marissa G. Coschigano, Eric A. Marro,† Ruoxi Li, Sydney L. Gregory, Alexandra F. Gittens, Maxime A. Siegler and Rebekka S. Klausen *

Received 31st March 2026,
Accepted 15th April 2026

DOI: 10.1039/d6dt00742b

rsc.li/dalton

The poly(cyclosilane)s are a class of hybrid inorganic–organic polymers with an all Si–Si backbone, arranged into repeating cyclohexasilane motifs, and mixed methyl and hydro side chains. The synthesis of a densely functionalized cyclosilane with three-fold symmetry enabled copolymerization studies yielding poly(cyclosilane)s with variable amounts of branching. The properties of the novel branched poly(cyclosilane)s were investigated and it was found that branching led to less volatilization during pyrolysis in an inert atmosphere, suggesting the utility of poly(cyclosilane)s for applications as preceramic polymers.

Introduction

Certain inorganic and hybrid inorganic–organic polymers, termed preceramic polymers, have distinctive thermal reactivity relative to organic polymers.[1–3] While organic polymers like poly(methyl methacrylate)[4] and polystyrene[5] depolymerize to monomer if heated to the appropriate temperature under an inert atmosphere, a preceramic polymer undergoes a series of thermal reactions (*e.g.*, cross-linking) that ultimately form high-performance ceramics. A landmark example was the Yajima process, in which pyrolysis of poly(dimethylsilane) (poly($SiMe_2$)) afforded a polycarbosilane intermediate that ultimately fused to high tensile strength silicon carbide (β-SiC) fibers.[6] The synthesis of hybrid inorganic–organic polymers sampling more of the periodic table enabled access to ceramics with a broad array of elemental compositions, such as poly(vinylboranes) affording boron carbide,[7–9] cyclosilazanes affording silicon nitride,[10–12] and zirconium-modified polyborasilazane for Si–B–C–N–Zr multinary ceramics.[13] An advantage of polymeric precursors is viscosity; a fluid polymer (or solid polymer soluble in organic solvent) can be molded, then fired, enabling the preparation of ceramic forms difficult to prepare from powder precursors. For example, porous polymer-derived ceramics (PDCs) can be used in catalytic reactions as supports. The combination of preceramic polymers with additive manufacturing techniques (*e.g.*, 3-D or 4-D printing) leads to critical components for extreme environments, such as aerospace.[14]

While there has been significant research on expanding the representation of the periodic table in preceramic polymers, limited synthetic control over macromolecular structure limits an understanding of how polymer microstructure and architecture affect ceramization. With respect to polysilane to silicon carbide, the ability to vary side chain structure in the polymerization of either R_2SiCl_2 or $RSiH_3$ precursors has provided some insights. Methyl groups are preferred over longer alkyl chains, as excess carbon in the precursor can lead to off-stoichiometry, carbon-rich ceramics.[15] A side chain proton is also advantageous for cross-linking.[15,16] Cyclic substructures (*e.g.*, Si_3N_3 and Si_4N_4 rings) are advantageous in the formation of silicon nitride.[17,18]

In combination, these insights suggest that the poly(cyclosilane)s[19–23] (*e.g.*, *lin*-poly(**1,3-Si$_6$**), Fig. 1a) could be compelling precursors to SiC given the combination of cyclic repeat units and mixed methyl and hydro side chains. We previously reported that a macrocyclic poly(cyclosilane) afforded higher char yields than a linear variant with the same constitutional repeat unit, which was attributed to the necessity of cleaving at least two Si–Si bonds to produce low molecular weight, poten-

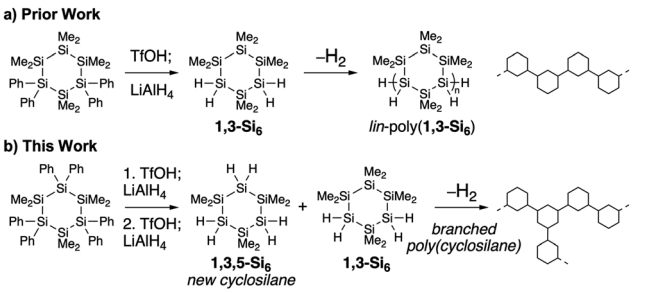

Fig. 1 (a) Prior work: synthesis of **1,3-Si$_6$** and dehydropolymerization to linear homopolymer.[19] (b) This work: synthesis of 1,3,5-hydrocyclohexasilane and dehydrocoupling polymerization yielding branched copolymer.

Department of Chemistry, Johns Hopkins University, 3400 N. Charles St, Baltimore, MD 21218, USA. E-mail: klausen@jhu.edu

†Current Address: Thermo Fischer, 1 Reagent Lane, Fair Lawn NJ 07410.

tially volatile fragments.[24] While promising, cyclic polymers are a significant synthetic challenge and are frequently contaminated with linear polymer.[25]

A branched poly(cyclosilane) architecture could afford some of the same advantages with respect to yield, as a single bond scission event could still afford high molecular weight material, but *via* a potentially more straightforward synthetic process. Examples of branched polysilanes are relatively limited,[26] but work on other preceramic polymers including polycarbosilanes (Si–C backbone) indicates branching increases ceramic yield.[27,28]

We sought to synthesize novel branched poly(cyclosilane)s to elucidate how branching affects pyrolysis, as well as other aspects of poly(cyclosilane) properties such as absorbance spectroscopy. Given our success in achieving dehydropolymerization of bifunctional cyclosilanes like **1,3-Si$_6$**, we targeted the trifunctional cyclosilane **1,3,5-Si$_6$** as a comonomer that could afford branched poly(cyclosilane)s (Fig. 1b). Cyclosilanes as densely functionalized as this are not well-known. A 1,3,5-hypersilyl cyclohexasilane molecule was synthesized by Marschner *et al. via* annulation of an α,ω-dipotassiooligosilyl dianion and ditriflate-neopentasilane,[29] but this functionalization pattern was not suitable for the formation of hydrofunctionalized cyclosilanes for dehydrocoupling.

Herein, we report the synthesis and characterization of novel cyclosilane **1,3,5-Si$_6$** *via* annulation and dearylation. The six-fold dearylation proved particularly challenging and we report a successful iterative approach to deprotection. Achieving this molecular synthesis enabled the synthesis of two novel copolymers with different amounts of branching arising from changes in the monomer feed ratio. The branched copolymers showed elevated char yields during pyrolysis.

Results and discussion

Synthesis of 1,3,5-Si$_6$

We hypothesized that an annulation between known nucleophilic oligosilyl dianion **1**[30] and known electrophilic α,ω-dichlorooligiosilane **2**[31] (Fig. 2a) should provide a cyclohexasilane **3** with the appropriate functionalization pattern. We previously reported the synthesis and the crystal structure of **1** determined by single crystal X-ray diffraction (SCXRD),[30,32] as well as other phenyl-substituted α,ω-dipotassiooligosilyl dianions with up to 5 contiguous silicon atoms.[19,20,33,34] While prior syntheses of **2** based on radical chlorination of a Si–H bond had been reported,[31,35] the low yield motivated us to develop the alternative synthesis shown in Fig. 2b, which provided **2** in 54% yield over two steps.

The annulation between **1** and **2** proceeded cleanly after K/Mg exchange with $MgBr_2{\cdot}OEt_2$, affording $(SiMe_2)_3(SiPh_2)_3$ (**3**) in 43% yield. The crystal structure of **3** was determined and showed a chair-like conformation of the central ring (Fig. 2c).

Conversion of **3** to **1,3,5-Si$_6$** would require converting the six phenyl rings to hydrogens. In our prior syntheses of tetrafunctional cyclosilanes (*e.g.*, **1,3-Si$_6$** and **1,4-Si$_6$**), this was accomplished in a two-step sequence of trifluoromethanesulfonic acid-mediated (TfOH) dearylation followed by $LiAlH_4$ reduction to a hydrosilane (*e.g.*, Si–Ph → Si–OTf → Si–H).[19,20] In these syntheses, we removed a maximum of four benzene rings in a single step[19,20] and a review of the literature raised concern that it would be challenging to remove six without undesired Si–Si bond cleavage. The TfOH-promoted conversion of a phenylsilane to a silyl triflate[36] and benzene is an example of an *ipso*-selective electrophilic aromatic substitution. As shown by Matyjaszewski in oligosilanes with more than one phenyl ring, the rate-determining step is protonation of the aryl ring; the first protonation is much faster than a second, as a silyl triflate deactivates a proximal phenylsilane.[37,38] While this effect can result in synthetically useful regioselectivities in polyarylsilanes, at sufficiently high conversions, Si–Ph protonation is deactivated to the point that Si–Si protonation is competitive and oligosilane backbone cleavage occurs.[39] We have previously observed failure to remove eight aryl rings in a ladder tricyclosilane.[40]

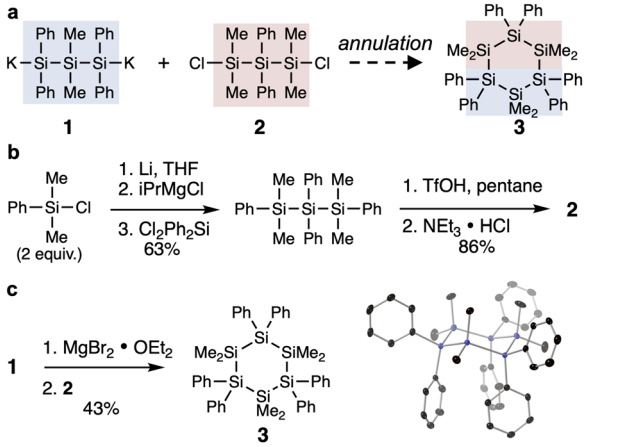

Fig. 2 (a) Proposed annulation to **3**. (b) Synthesis of **2**. (c) Synthesis of **3** and displacement ellipsoid plot (50% probability) of one of the two crystallographically independent molecules of **3** at 110 K. Blue = silicon, black = carbon. Hydrogens omitted are for clarity.

Indeed, our attempts to convert $(SiMe_2)_3(SiPh_2)_3$ **3** to $(SiMe_2)_3(SiOTf_2)_3$ in a single step failed under a variety of conditions (Fig. 3a and Fig. S1). Inspired by a report from Haas *et al.*,[41] we instead focused on an iterative approach, in which removal of three aryl rings would form intermediate **4**, which after a second iteration of protonation and reduction would afford **1,3,5-Si$_6$** (Fig. 3b). We expected **4** instead of another skeletal isomer because of the triflate deactivating effect discussed above, which ensures regioselective distal protonation rather than geminal protonation in diarylsilanes.[37]

The first threefold-dearylation (3.3 equiv. TfOH, 0 °C) was investigated in a variety of solvents. Prior work has suggested that ionization of silyl triflates can lead to skeletal rearrangement *via* formation of transient silylium ions.[42–44] We therefore sought a solvent that could dissolve crystalline **3**, while

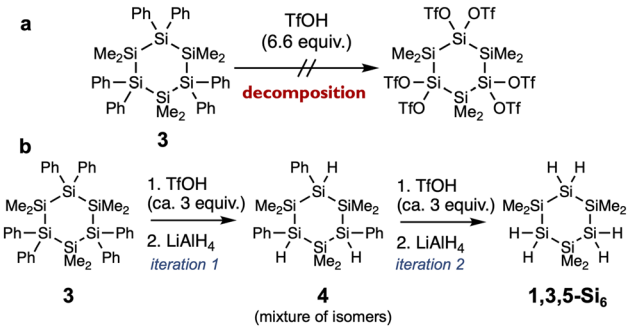

Fig. 3 (a) Failed six-fold dearylation. (b) Proposed iterative dearylation–reduction.

being sufficiently nonpolar to minimize skeletal rearrangement. We identified toluene as a promising candidate (Table 1). As the intermediate tri-triflate was hydrolytically sensitive, it was immediately reduced to **4**. Both lithium aluminium hydride (LAH) and diisobutylaluminum hydride (DIBAL)[41] were tested as reducing agents, where LAH resulted in the cleanest material. Thus, over two steps, **3** was successfully converted to **4** as a mixture of diastereomers in an unpurified yield of 76% after removal of inorganic byproducts.

During attempted purification of **4**, the *cis*,*cis* diastereomer selectively crystallized from toluene, a phenomenon previously observed for *cis*,*cis*-1,3,5-trihydroxynonamethylcyclohexasilane attributed to isomeric differences in polarity and therefore solubility in organic solvents.[45] As seen in the crystal structure determined by SCXRD (Fig. 4a), the cyclohexasilane core adopted a chair-like conformation with the phenyl groups in the equatorial position. The single isomer was also characterized by ^{1}H NMR spectroscopy (Fig. 4b), where the high symmetry of *cis*,*cis*-**4** is apparent. While the *cis*,*cis* diastereomer could account for up to 46% of all isomers of **4** present, as determined by ^{1}H NMR spectroscopy, the achieved isolated

Table 1 Variation in solvent and hydride donor in conversion of **3** to **4**

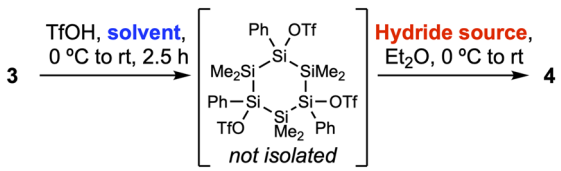

Entry	Solvent	Hydride source	Yield[a] (%)
1	Pentane	LAH	Decomposition
2	Toluene	LAH	76
3	Benzene	LAH	35
4	CH_2Cl_2	LAH	Decomposition
5	Toluene	DIBAL	Complex mixture[b]
6	Benzene	DIBAL	Complex mixture[b]

[a] Yield is of all combined diastereomers and is reported over two steps (**3** → **4**) and after removal of inorganic byproducts. [b] Compound **4** was not isolated.

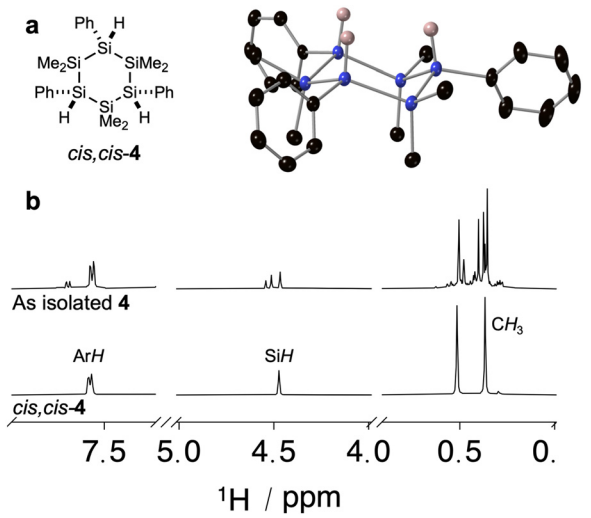

Fig. 4 (a) Molecular structure and displacement ellipsoid plot (50% probability level) at 110 K of *cis*,*cis*-**4**. Hydrogen atoms (except for the Si–H) are omitted for clarity. Blue = silicon, black = carbon, pink = hydrogen. (b) Cropped ^{1}H NMR spectra (400 MHz, C_6D_6) of as isolated **4** and the crystalline diastereomer *cis*,*cis*-**4**.

yield of the single diastereomer was 15%. While the crystal structure established confidence in the lack of skeletal rearrangement, the low yield was not conducive to a high throughput synthesis of **1,3,5-Si$_6$** and we carried forward the as synthesized mixture of diastereomers without further purification.

The second iteration of dearylation–reduction to convert **4** to **1,3,5-Si$_6$** proved more challenging. Decomposition was observed with the conditions that proved successful for **3** to **4** (Fig. S1). Ultimately, we found that decreasing the temperature at which dearylation was performed from 0 °C to −78 °C reduced the quantity of undesired decomposition byproducts. At this lower temperature, the reaction time needed to be extended from 2.5 hours to 15 hours. Even with the long reaction time, incomplete consumption of the phenyl groups was observed *via* ^{1}H NMR spectroscopy with standard amounts of TfOH (*e.g.*, 1.1 equiv. per phenyl ring) (Fig. S2). Increasing the amount of TfOH to 1.5 equiv. per phenyl ring resulted in full conversion of the phenyl groups. The typical reduction conditions were sufficient for conversion of the intermediate tri-triflate to **1,3,5-Si$_6$** (Fig. 5a). After removal of lithium salts and vacuum distillation, **1,3,5-Si$_6$** was isolated as a clear, colorless oil in 7% yield over four steps beginning from **3**. Characterization *via* ^{1}H, ^{13}C, and ^{29}Si NMR spectroscopy (Fig. 5b–d) verified isolation of the desired highly symmetric product.

Copolymerizations

With **1,3,5-Si$_6$** in hand, we turned towards copolymerization with **1,3-Si$_6$** (Scheme 1), where we expected trifunctional **1,3,5-Si$_6$** would introduce branches into the polymer chain.

Copolymerization of **1,3-Si$_6$** and **1,3,5-Si$_6$** was carried out under the conditions previously used for cyclosilane homopo-

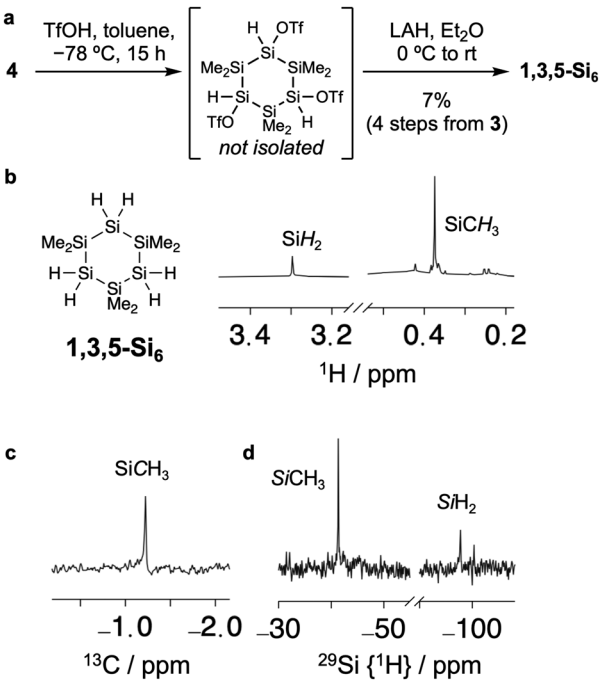

Fig. 5 (a) Dearylation and reduction of cyclosilane **4**. (b) Cropped ^{1}H NMR spectrum (400 MHz, C_6D_6) of **1,3,5-Si$_6$**. (c) Cropped ^{13}C {^{1}H} dec30 NMR spectrum (400 MHz, C_6D_6) of **1,3,5-Si$_6$**. (d) Cropped ^{29}Si {^{1}H} DEPT NMR spectrum (400 MHz, C_6D_6) of **1,3,5-Si$_6$**.

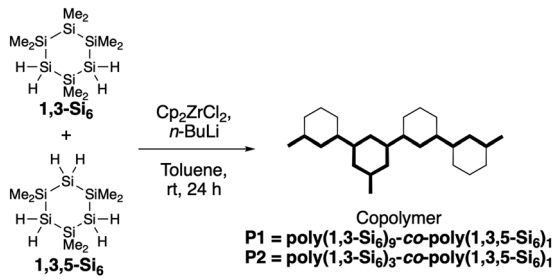

Scheme 1 Copolymerization of cyclosilanes **1,3-Si$_6$** and **1,3,5-Si$_6$** to 10% and 25% copolymers **P1** and **P2** respectively.

lymer formation,[19,20,22] derived from well-established dehydrogenative coupling procedures using the Cp_2ZrCl_2/*n*-BuLi catalytic system.[46,47] Monomer loadings of 10 and 25 mol% of **1,3,5-Si$_6$** were used to form **P1** and **P2**, respectively (Scheme 1). Complete consumption of monomers was observed by ^{1}H NMR spectra (Fig. S3). The copolymers were less soluble in pentane than **1,3-Si$_6$** homopolymers. In prior work, dissolution of the polymer in pentane followed by Celite filtration[20] was employed to remove residual zirconocene catalyst. In this case, filtration resulted in decreased molecular weight by size exclusion chromatography (SEC) when compared to the unpurified sample (Fig. S4). We suggest that solubility in pentane decreases with increased branching,[48] which results in separation of the more soluble linear **1,3-Si$_6$** homopolymer components. Aside from lower solubility in pentane, no physical differences were observed between the branched copolymers and linear homopolymers.

The SEC elugrams of the branched polymers **P1** and **P2**, without Celite filtration, relative to unbranched *lin*-poly(**1,3-Si$_6$**) are shown in Fig. 6 and molecular weight characteristics are reported in Table 2. The previously reported *lin*-poly(**1,3-Si$_6$**) has a relatively unimodal and narrow distribution of molecular weights, corresponding to a dispersity of M_w/M_n = 1.40. With branching, the M_w, M_n, and dispersity all increased, and a pronounced shoulder was observed. These changes in molecular weight distribution are characteristic of branched polymers and have been attributed to changes in hydrodynamic volume,[49] rather than changes in degree of polymerization. The strands of the branched polymers are less able to tightly pack, resulting in a more open network[50] and larger hydrodynamic volume.

As there is no clear structural reason why the structure of **1,3,5-Si$_6$** might lead to an increased degree of polymerization, we instead interpret these data to reflect a branched copolymer with a likely primary chain length similar to the homopolymer. This is supported by both the trend of an apparent increased molecular weight with increasing concentration of **1,3,5-Si$_6$** in the monomer feed, which would result in more branching, and an observed broadening in ^{1}H NMR spectra (Fig. S5).

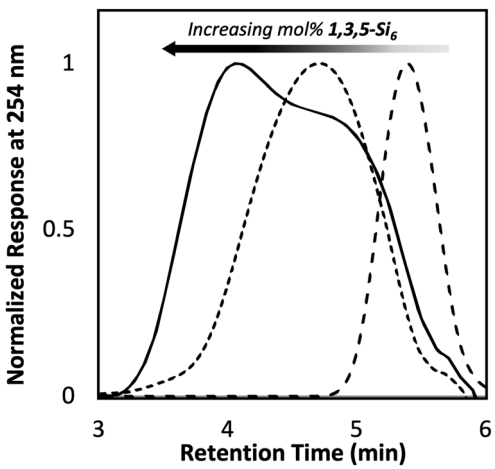

Fig. 6 Normalized SEC curves of *lin*-poly(**1,3-Si$_6$**) (dashed), **P1** (dotted), and **P2** (solid).

Table 2 Molecular weight characteristics of copolymers

Polymer	**1,3,5-Si$_6$** (mol%)	M_n [a] (g mol^{-1})	M_w [a] (g mol^{-1})	M_w/M_n
lin-**Poly(1,3-Si$_6$)**	0	1920	2690	1.40
P1	10	7220	23 200	3.21
P2	25	7050	52 980	7.52

[a] Determined by size exclusion chromatography relative to polystyrene standards at 254 nm (THF, [polymer] = 1 mg mL^{-1}, 40 °C, 0.35 mL min^{-1}, 10 μL injection).

UV-Vis spectroscopy

Polysilanes are distinct from the homologous polyolefins in absorbing UV light, typically between 250–350 nm.[51] Due to σ-conjugation, the absorption properties of the polymers are red-shifted relative to monomers.[21] We therefore collected UV-vis spectra of the small molecules **3**, *cis*,*cis*-**4**, and **1,3,5-Si$_6$** (Fig. 7a), as well as all copolymers (Fig. 7b).

The spectra of **3** and *cis*,*cis*-**4**, which differ in the number of phenyl substituents, were overall very similar with respect to the wavelength of maximum absorption (λ_{max}, Table 3). The narrower width of the *ca.* 255 nm transition in *cis*,*cis*-**4** relative to **3** (Fig. 7a) may reflect a less conformationally dynamic structure due to a preference to place the bulkier phenyl substituents in the equatorial positions. Constraining oligosilane conformation whether through structural changes or low temperatures tends to result in narrower absorption bands[52] and oligosilanes are well-known to exhibit conformation-dependent UV-vis spectra.[21,52–54] The spectrum of cyclosilane **1,3,5-Si$_6$** was observed to be very similar to **1,3-Si$_6$** and **1,4-Si$_6$** in exhibiting a λ_{max} <200 nm, with an onset of absorption *ca.* 230 nm. Overall, the spectrum of **1,3,5-Si$_6$** is consistent with σ–σ* transitions, while the spectra of **3** and *cis*,*cis*-**4** reflect contributions from orbitals of both σ (the cyclosilane) and π symmetry (the phenyl substituents).

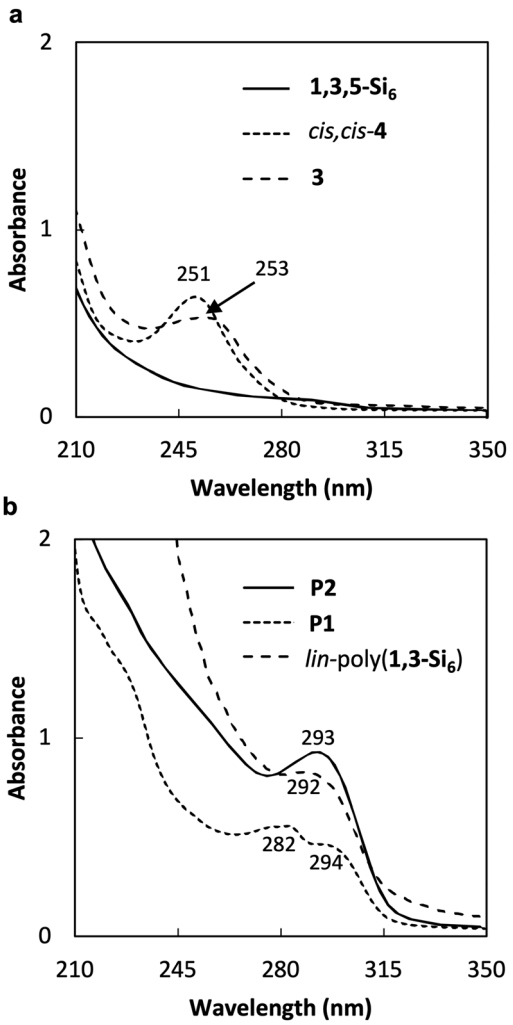

Fig. 7 UV-vis spectra of (a) small molecules **3**, *cis*,*cis*-**4**, and **1,3,5-Si$_6$** ([compound] = 3.00 × 10^{-5} M, in pentane) and (b) polymers *lin*-poly(**1,3-Si$_6$**), **P1**, and **P2** ([polymer] = 0.012 mg mL^{-1}, THF).

Table 3 Wavelength of maximum absorbance (λ_{max}) for cyclosilanes[a] and poly(cyclosilane)s[b]

Molecule		λ_{max} (nm)	
3		<190	
cis,*cis*-**4**		251	
1,3,5-Si$_6$		253	
Polymer	**1,3,5-Si$_6$** (mol%)	λ_{max} (nm)	λ_{onset} (nm)
lin-**Poly(1,3-Si$_6$)**	0	292	308
P1	10	294	317
P2	25	293	317

[a] Conditions: [compound] = 3.00 × 10^{-5} M, in pentane. [b] Conditions: [polymer] = 0.012 mg mL^{-1}, THF.

Polymerization of **1,3,5-Si$_6$** resulted in a substantial red-shift in copolymer absorption relative to monomers (<190 nm to *ca.* 295 nm, Fig. 7 and Table 3). The copolymers **P1** and **P2** were overall similar to each other and to unbranched homopolymer *lin*-poly(**1,3-Si$_6$**) (Fig. 7b and Table 3). These data suggest that branching does not perturb the σ-conjugation length in the poly(cyclosilane).[55]

Thermal properties

The thermal ceramization of polydimethylsilane (poly(SiMe$_2$)) to silicon carbide proceeds in two stages. Pyrolysis at *ca.* 400 °C converts the polysilane to a polycarbosilane (Fig. 8a). The intermediate polycarbosilane can be isolated. Low molecular weight, formable materials are desired so that specific shapes can be obtained before the resin is heated to even higher temperatures to afford the desired silicon carbide. A major challenge is managing mass loss; any material volatilized during either stage affects the overall yield of silicon carbide, as well as shrinkage.

A radical chain mechanism (Kumada rearrangement)[56] for the polysilane to polycarbosilane reaction has been proposed (Fig. 8b) and suggests explanations for the low yield. Initiation occurs *via* homolysis of the polysilane backbone, forming two silyl radicals (**A**). Abstraction of a hydrogen from an adjacent side chain affords a primary alkyl radical **B** and hydrogen-terminated polymer chain. A major contributor to mass loss and low yield is *via* the silyl macroradical **A**, which can competitively depolymerize *via* back-biting to yield low molecular weight and volatile cyclic byproducts. Rearrangement of the primary alkyl radical **B** inserts carbon into the Si–Si backbone and forms a new silyl radical **C**, which can abstract hydrogen from another methyl side chain to regenerate **B** and propagate the radical chain reaction.

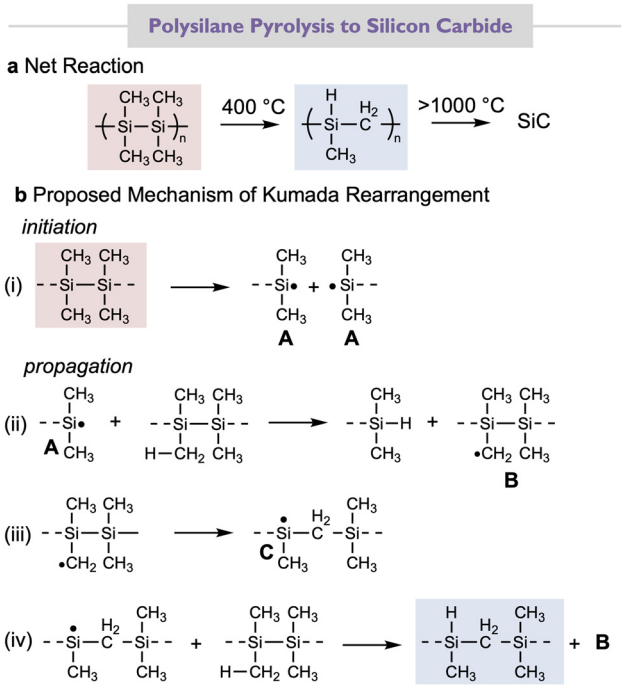

Fig. 8 Summary of prior work on polydimethylsilane pyrolysis to silicon carbide. (a) Net reaction: ceramization occurs *via* skeletal rearrangement, followed by increased heating to yield silicon carbide. (b) Proposed mechanism of radical rearrangement of polysilane to polycarbosilane during pyrolysis *via* Kumada rearrangement.

Thermogravimetric analysis (TGA) is an established method for investigating the relationship between temperature and mass loss during the polysilane to polycarbosilane process. We have also previously studied the thermal reactivity of linear and cyclic poly(cyclosilane)s and TGA analysis of *lin*-poly(**1,3-Si$_6$**) is reproduced in Fig. 9 (blue). The dashed line is percentage weight change, and the solid line is the derivative weight change. A change in weight begins at *ca.* 200 °C and was assigned to Si–Si bond cleavage, as supported by density functional theory calculations of the bond dissociation energies of the cyclosilane microstructure which suggested the Si–Si bonds between cyclosilanes are weaker than not only other Si–Si bonds, but also Si–H or Si–C bonds. A second phase of weight change was observed at *ca.* 400–500 °C and was assigned to thermal curing *via* dehydrogenation (*e.g.*, H_2 loss) leading to radical–radical crosslinking between chains.

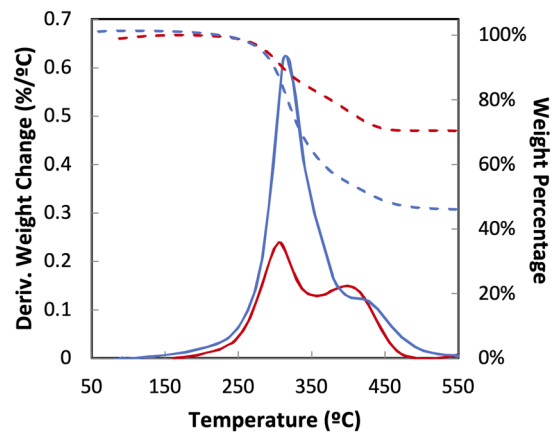

Fig. 9 TGA curves of *lin*-poly(**1,3-Si$_6$**)[24] (blue) and **P2** (red). Solid lines: derivative weight change; dotted lines: percentage weight change.

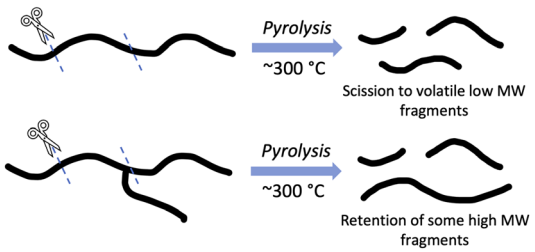

Fig. 10 Graphic illustrating retention of higher molecular weight fragments after Si–Si bond scission during pyrolysis of branched polymers (lower) compared to forming volatile low molecular weight fragments from linear polymers (upper).

We assessed the thermal decomposition behavior from 40 to 600 °C of the branched poly(cyclosilane)s **P1** and **P2** relative to the linear poly(**1,3-Si$_6$**).[24] For **P1**, high quality data could not be attained. A consistent increase in mass was observed until 500 °C, possibly due to autooxidation from residual Si–H bonds. When comparing **P2** (red) to unbranched *lin*-poly(**1,3-Si$_6$**) much less mass loss was observed in the initial 200–300 °C phase. In contrast, the derivative weight change around 400 °C assigned to dehydrogenation and crosslinking remained fairly consistent across both polymers.[57]

These data are consistent with branched polymers affording fewer volatile byproducts than unbranched. We hypothesize that when Si–Si homolysis occurs between cyclosilanes in a branched architecture, rather than forming volatile small molecules, higher molecular weight chains are retained that can continue to form polycarbosilane, as visually depicted in Fig. 10.

Overall, the reduced volatilization resulted in an increase in char yield from 45% to 70% from the linear to the branched copolymer, a nearly two-fold increase in yield.

Conclusion

The successful design and synthesis of inherently branched trifunctional cyclohexasilane monomer **1,3,5-Si$_6$** *via* iterative dearylation afforded access to two poly(cyclosilane)s with differing degrees of branching. The effect of branched microstructure on thermal behaviour was assessed. Our results suggest that cyclic substructures and branched architectures increase yield in poly(cyclosilane) pyrolysis. These results provide design principles enhancing the utility of inorganic polymers as precursors for the formation of high-performance ceramics.

Conflicts of interest

There are no conflicts of interest to declare.

Data availability

The data supporting this article have been included as part of the supplementary information (SI). Experimental procedures, spectroscopic data, supplemental figures. See DOI: https://doi.org/10.1039/d6dt00742b.

CCDC 2541080 and 2541081 contain the supplementary crystallographic data for this paper.[58a,b]

Acknowledgements

This research was primarily supported by the U.S. Department of Energy (DOE), Office of Science, Basic Energy Sciences, under Award No. DE-SC0020681. Single crystal X-ray crystallography was supported by the U.S. National Institutes of Health (NIH) under Award 1S10OD030352 (M. A. S).

References

1 R. M. Laine and F. Babonneau, *Chem. Mater.*, 1993, **5**, 260–279.
2 B. J. Ackley, K. L. Martin, T. S. Key, C. M. Clarkson, J. J. Bowen, N. D. Posey, J. F. Ponder Jr., Z. D. Apostolov, M. K. Cinibulk, T. L. Pruyn and M. B. Dickerson, *Chem. Rev.*, 2023, **123**, 4188–4236.
3 M. Birot, J.-P. Pillot and J. Dunogues, *Chem. Rev.*, 1995, **95**, 1443–1477.
4 G. R. Jones, H. S. Wang, K. Parkatzidis, R. Whitfield, N. P. Truong and A. Anastasaki, *J. Am. Chem. Soc.*, 2023, **145**, 9898–9915.
5 W. Kaminsky, *Makromol. Chem., Macromol. Symp.*, 1991, **48–49**, 381–393.
6 S. Yajima, J. Hayashi, M. Omori and K. Okamura, *Nature*, 1976, **261**, 683–685.
7 M. G. L. Mirabelli and L. G. Sneddon, *J. Am. Chem. Soc.*, 1988, **110**, 3305–3307.
8 D. Seyferth, W. S. Rees, J. S. Haggerty and A. Lightfoot, *Chem. Mater.*, 1989, **1**, 45–52.
9 W. Li, J. Ding, Z. Yu and R. Riedel, *Mater. Today*, 2025, **90**, 882–910.
10 D. Seyferth, G. H. Wiseman and C. Prud'homme, *J. Am. Ceram. Soc.*, 1983, **66**, C13–C14.
11 N. R. Dando, A. J. Perrotta, C. Strohmann, R. M. Stewart and D. Seyferth, *Chem. Mater.*, 1993, **5**, 1624–1630.
12 D. Fonblanc, D. Lopez-Ferber, M. Wynn, A. Lale, A. Soleilhavoup, A. Leriche, Y. Iwamoto, F. Rossignol, C. Gervais and S. Bernard, *Dalton Trans.*, 2018, **47**, 14580–14593.
13 X. Long, C. Shao, H. Wang and J. Wang, *Dalton Trans.*, 2015, **44**, 15463–15469.
14 S. Khuje, N. Ku, A. Bujanda, J. Yu, H. Tsang, N. Meuse, L. Vargas-Gonzalez and S. Ren, *npj Adv. Manuf.*, 2026, **3**, 8.
15 Z. Zhang, F. Babonneau, R. M. Laine, Y. Mu, J. F. Harrod and J. A. Rahn, *J. Am. Ceram. Soc.*, 1991, **74**, 670–673.
16 X. Cheng, Z. Xie, Y. Song, J. Xiao and Y. Wang, *J. Appl. Polym. Sci.*, 2006, **99**, 1188–1194.
17 C. Xu, C. Liu, Z. Zheng, Y. Li, Z. Zhang, S. Yang and Z. Xie, *J. Appl. Polym. Sci.*, 2001, **82**, 2827–2831.
18 Y. D. Blum, K. B. Schwartz and R. M. Laine, *J. Mater. Sci.*, 1989, **24**, 1707–1718.
19 E. A. Marro, E. M. Press, M. A. Siegler and R. S. Klausen, *J. Am. Chem. Soc.*, 2018, **140**, 5976–5986.
20 E. M. Press, E. A. Marro, S. K. Surampudi, M. A. Siegler, J. A. Tang and R. S. Klausen, *Angew. Chem., Int. Ed.*, 2017, **56**, 568–572.
21 F. Fang, Q. Jiang and R. S. Klausen, *J. Am. Chem. Soc.*, 2022, **144**, 7834–7843.
22 C. P. Folster and R. S. Klausen, *Polym. Chem.*, 2018, **9**, 1938–1941.
23 E. A. Marro, C. P. Folster, E. M. Press, H. Im, J. T. Ferguson, M. A. Siegler and R. S. Klausen, *J. Am. Chem. Soc.*, 2019, **141**, 17926–17936.
24 Q. Jiang, S. Wong and R. S. Klausen, *Polym. Chem.*, 2021, **12**, 4785–4794.
25 T.-W. Wang and M. R. Golder, *Polym. Chem.*, 2021, **12**, 958–969.
26 K. Deller and B. Rieger, *RSC Adv.*, 2015, **5**, 87445–87455.
27 C. L. Schilling, J. P. Wesson and T. C. Williams, *J. Polym. Sci., Polym. Symp.*, 1983, **70**, 121–128.
28 C. K. Whitmarsh and L. V. Interrante, *Organometallics*, 1991, **10**, 1336–1344.
29 A. Wallner, J. Hlina, T. Konopa, H. Wagner, J. Baumgartner, C. Marschner and U. Flörke, *Organometallics*, 2010, **29**, 2660–2675.
30 H. Wakefield, I. Kevlishvili, K. E. Wentz, Y. Yao, T. B. Kouznetsova, S. J. Melvin, E. G. Ambrosius, A. Herzog-Arbeitman, M. A. Siegler, J. A. Johnson, S. L. Craig, H. J. Kulik and R. S. Klausen, *J. Am. Chem. Soc.*, 2023, **145**, 10187–10196.
31 A. G. Moiseev and W. J. Leigh, *J. Am. Chem. Soc.*, 2006, **128**, 14442–14443.
32 H. Wakefield, S. J. Melvin, J. Jiang, I. Kevlishvili, M. A. Siegler, S. L. Craig, H. J. Kulik and R. S. Klausen, *Chem. Commun.*, 2024, **60**, 4842–4845.
33 E. A. Marro, E. M. Press, T. K. Purkait, D. Jimenez, M. A. Siegler and R. S. Klausen, *Chem. – Eur. J.*, 2017, **23**, 15633–15637.
34 T. K. Purkait, E. M. Press, E. A. Marro, M. A. Siegler and R. S. Klausen, *Organometallics*, 2019, **38**, 1688–1698.
35 Y. Pang, S. A. Petrich, V. G. Young, M. S. Gordon and T. J. Barton, *J. Am. Chem. Soc.*, 1993, **115**, 2534–2536.
36 W. Uhlig and A. Tzschach, *J. Organomet. Chem.*, 1989, **378**, C1–C5.
37 K. Matyjaszewski and Y. L. Chen, *J. Organomet. Chem.*, 1988, **340**, 7–12.
38 K. E. Ruehl and K. Matyjaszewski, *J. Organomet. Chem.*, 1991, **410**, 1–12.

39 E. Fossum, S. W. Gordon-Wylie and K. Matyjaszewski, *Organometallics*, 1994, **13**, 1695–1698.
40 F. Fang, A. Molino, K. E. Wentz, C. P. Folster, J. L. Williams, M. A. Siegler and R. S. Klausen, *Angew. Chem., Int. Ed.*, 2025, **64**, e202506054.
41 V. Christopoulos, M. Rotzinger, M. Gerwig, J. Seidel, E. Kroke, M. Holthausen, O. Wunnicke, A. Torvisco, R. Fischer, M. Haas and H. Stueger, *Inorg. Chem.*, 2019, **58**, 8820–8828.
42 C. Krempner, U. Jäger-Fiedler, C. Mamat, A. Spannenberg and K. Weichert, *New J. Chem.*, 2005, **29**, 1581.
43 J. Y. Corey, D. M. Kraichely, J. L. Huhmann and J. Braddock-Wilking, *Organometallics*, 1994, **13**, 3408–3410.
44 J. Y. Corey, D. M. Kraichely, J. L. Huhmann, J. Braddock-Wilking and A. Lindeberg, *Organometallics*, 1995, **14**, 2704–2717.
45 H. Stueger, J. Albering, M. Flock, G. Fuerpass and T. Mitterfellner, *Organometallics*, 2011, **30**, 2531–2538.
46 E.-I. Negishi and T. Takahashi, *Acc. Chem. Res.*, 1994, **27**, 124–130.
47 J. Y. Corey and Z. Xiao-Hong, *J. Organomet. Chem.*, 1992, **439**, 1–17.
48 G. Shao, A. Li, Y. Liu, B. Yuan and W. Zhang, *Macromolecules*, 2024, **57**, 830–846.
49 S. Zhu, *Macromolecules*, 1998, **31**, 7519–7527.
50 Y. Braeken, S. Cheruku, S. Seneca, N. Smisdom, L. Berden, L. Kruyfhooft, H. Penxten, L. Lutsen, E. Fron, D. Vanderzande, M. Ameloot, W. Maes and A. Ethirajan, *ACS Biomater. Sci. Eng.*, 2019, **5**, 1967–1977.
51 R. S. Klausen and E. Ballestero-Martínez, in *Comprehensive Organometallic Chemistry IV*, Elsevier, 2022, pp. 135–165.
52 A. Fukazawa, H. Tsuji and K. Tamao, *J. Am. Chem. Soc.*, 2006, **128**, 6800–6801.
53 K. Tamao, H. Tsuji, M. Terada, M. Asahara, S. Yamaguchi and A. Toshimitsu, *Angew. Chem., Int. Ed.*, 2000, **39**, 3287–3290.
54 H. Tsuji, H. A. Fogarty, M. Ehara, R. Fukuda, D. L. Casher, K. Tamao, H. Nakatsuji and J. Michl, *Chem. – Eur. J.*, 2014, **20**, 9431–9441.
55 H. Tsuji, M. Terada, A. Toshimitsu and K. Tamao, *J. Am. Chem. Soc.*, 2003, **125**, 7486–7487.
56 K. Shiina and M. Kumada, *J. Org. Chem.*, 1958, **23**, 139.
57 M. G. Coschigano, S. L. Gregory, J. Catazaro, A. J. Rossini and R. S. Klausen, *Macromolecules*, 2024, **57**, 4095–4106.
58 (*a*) CCDC 2541080: Experimental Crystal Structure Determination, 2026, DOI: 10.5517/ccdc.csd.cc2r96bm; (*b*) CCDC 2541081: Experimental Crystal Structure Determination, 2026, DOI: 10.5517/ccdc.csd.cc2r96cn.